2009

Magnetic Hole Formation from the Perspective of Inverse Scattering Theory

Robert L. Hamilton
George Fox University, rhamilto@georgefox.edu

D A. Peterson
George Fox University

S M. Libby
George Fox University

Magnetic hole formation from the perspective of inverse scattering theory

R. L. Hamilton,[1] D. A. Peterson,[1] and S. M. Libby[1]

[1] The dynamics of oblique, weakly dispersive nonlinear Alfven waves in the presence of weak resistive damping are investigated numerically through an extension of the derivative nonlinear Schrodinger (DNLS) equation. It is observed numerically that the nonlinear dynamics are organized around the dynamics and allowed interactions of the underlying DNLS soliton families. There are three types of oblique Alfven solitons: the compressive two-parameter soliton and one-parameter bright soliton along with the rarefactive one-parameter dark soliton. The damping of either of these compressive solitons is accompanied by the formation of one or more dark solitons. The implication of these processes is that any initial wave profile containing solitons in its Inverse Scattering Transformation representation, in the presence of weak resistive damping, will result in a leading train of dark solitons. These dark solitons have been identified with magnetic holes, and the results described above are discussed in the context of magnetic hole observations and theory.

Citation: Hamilton, R. L., D. A. Peterson, and S. M. Libby (2009), Magnetic hole formation from the perspective of inverse scattering theory, *J. Geophys. Res.*, *114*, A03104, doi:10.1029/2008JA013582.

1. Introduction

[2] The dynamics of weakly dispersive, oblique Alfven waves in the presence of weak resistive damping is studied through a numerical solution of the derivative nonlinear Schrodinger-Burgers (DNLSB) model equation [*Wyller and Mjolhus*, 1984]. In the absence of dissipation the DNLSB reduces to the derivative nonlinear Schrodinger (DNLS) equation [*Rogister*, 1971; *Kennel et al.*, 1988] which is integrable through the Inverse Scattering Transformation (IST) [*Kaup and Newell*, 1978; *Kawata and Inoue*, 1978]. The IST is used as an aid in representing and interpreting the underlying nonlinear dynamics. For weak dissipation, the IST also provides simple constraints on the dynamics which allow the results to be extended to a broader class of Alfven wave profiles than are considered in this paper. The primary result found through this method is that Alfven wave profiles containing compressive solitons in their IST representation will evolve into a train of dark solitons if subject to weak resistive damping. This result is of specific interest in the context of magnetic holes which have a tentative relation to such dark solitons. It is conjectured that the IST may provide useful insights and constraints on the underlying nonlinear dynamics of Alfven waves in systems that can be considered as perturbations of the DNLS equation. Following, there is brief overview of magnetic hole observations, theories and the role of solitons in this context.

[3] Magnetic holes are localized reductions in the magnetic field that were identified in solar wind data early on by *Sugiura et al.* [1969] and by *Turner et al.* [1977]. Following these initial observations, magnetic holes have been observed in planetary magnetosheaths [*Erdos and Balogh*, 1996], the solar wind from 0.3 AU out to 17 AU [*Sperveslage et al.*, 2000], the magnetosheath of comet Halley [*Russell et al.*, 1987], as far out as 97 AU in the heliosheath [*Burlaga et al.*, 2006] and at very high heliocentric latitudes [*Tsurutani et al.*, 2002a, 2002b]. Typically magnetic holes occur with a direction of propagation nearly perpendicular to the ambient magnetic field and in regions of high β [*Sperveslage et al.*, 2000] but have also been observed in low-β environments [*Stasiewicz et al.*, 2003; *Stasiewicz*, 2004] as well as traveling at relatively small angles to the ambient magnetic field [*Tsurutani et al.*, 2002a, 2002b]. There may be a change in the direction of wave travel across a magnetic hole. If the change in direction is small, they are referred to as ''linear'' magnetic holes by *Turner et al.* [1977], who reported that 8 of the 28 magnetic holes they identified were linear holes. *Sperveslage et al.* [2000] reported that 30% of the 850 magnetic holes they identified were linear. It is reported that magnetic holes can be observed in isolation [*Turner et al.*, 1977] or appear in closely spaced trains [*Sugiura et al.*, 1969; *Winterhalter et al.*, 2000; *Tsurutani et al.*, 2002b; *Burlaga et al.*, 2006]. It has been noted that comparable observations of magnetic compression are rare, but do exist [*Sperveslage et al.*, 2000; *Turner et al.*, 1977; *Burlaga et al.*, 2006] and that these magnetic compressions tend to be either clustered or connected to field profiles similar to magnetic holes. Finally, *Tsurutani et al.* [2002a, 2002b, 2005] have observed that non-''linear'' magnetic holes are associated with phase

[1]Department of Engineering, Math and Computer Science, George Fox University, Newberg, Oregon, USA.

steepening related to the change in direction across the holes as well as proton perpendicular heating along with the presence of dissipation. While it is not expected that the diverse observational settings mentioned above can be accurately described as mere perturbations to the DNLS model equation, the dark soliton formation method described in this article does give a simple explanation for the occurrence of trains of magnetic holes and for the connection of relatively scarce compressive waves with such trains.

[4] In setting the framework for discussing the developing theory of magnetic holes, it seems helpful to make a distinction [*Baumgärtel*, 1999; *Sperveslage et al.*, 2000; *Winterhalter et al.*, 1994] between mechanisms that lead to the initial formation of magnetic holes and those that govern their subsequent evolution. In this context, the mirror mode instability has received much attention in observational [*Tsurutani et al.*, 1982, 1992; *Winterhalter et al.*, 1994; *Erdos and Balogh*, 1996; *Sperveslage et al.*, 2000; *Winterhalter et al.*, 2000; *Burlaga et al.*, 2006] as well as in theoretical and numerical studies [*Kivelson and Southwood*, 1996; *Pantellini*, 1998; *Baumgärtel et al.*, 2003] as a mechanism that could lead to the initial formation of magnetic holes. While the conditions for the linear mirror mode instability are closely correlated through satellite observations with the formation of magnetic holes, it has been noted [*Erdos and Balogh*, 1996; *Sperveslage et al.*, 2000] that this linear theory predicts an equal distribution of magnetic field compressions and depressions where observation shows a preference for magnetic field depressions. The nonlinear saturation of the mirror mode instability has been addressed theoretically [*Pantellini*, 1998; *Pokhotelov et al.*, 2008] and numerically [*Baumgärtel et al.*, 2003; *Califano et al.*, 2008] with conflicting results. The theoretical results of *Pokhotelov et al.* [2008] clearly show that the mirror instability leads to an unbounded depression in the magnetic field. They show that this instability may be quenched by the inclusion of particle trapping effects resulting in a magnetic field depression, a result generally in common with *Pantellini* [1998]. The numerical results of the 1-D hybrid code used by *Baumgärtel et al.* [2003] and *Califano et al.* [2008] indicate that the nonlinear mirror mode instability is not sufficient to yield the observed properties of short-scale magnetic holes but rather instead produces magnetic humps, or local increases in the magnetic field. In particular, *Califano et al.* [2008] point to the role of kinetic effects in thwarting even the initial formation of magnetic depressions. Their simulation shows that far from the threshold, the field transforms into magnetic holes. In this context, the soliton damping model discussed here can apply to the evolution of an initial nonlinear wave profile, but not the formation of nonlinear wave structures from a quiescent field as in the simulations mentioned above.

[5] The role of solitons in describing magnetic holes has been evaluated by several authors [*Baumgärtel*, 1999; *Sperveslage et al.*, 2000; *Baumgärtel et al.*, 2003; *Buti et al.*, 2001; *Stasiewicz et al.*, 2003; *Stasiewicz*, 2004] and is typically motivated, in part, as a means to account for their nonlinear character and apparent stability. A detailed discussion of related soliton equations and soliton properties was presented by *Mjolhus* [2006]. Of particular interest in this paper is the DNLS equation which has been derived as the one-dimensional, weakly nonlinear, weakly dispersive limit of Hall-MHD appropriate for wave travel parallel, or nearly parallel, to the ambient magnetic field for a plasma with $\beta < 1$ [*Kennel et al.*, 1988]. As discussed in section 2, under certain conditions the DNLS description of Alfven waves can be extended to large amplitude, oblique waves in a high-β plasma. It breaks down for oblique waves with $\beta < 1$ and so cannot be related to the works of *Baumgärtel et al.* [2005], *Stasiewicz et al.* [2003] or *Stasiewicz* [2004]. *Baumgärtel* [1999] found rarefactive DNLS solitons to be stable solutions of the Hall-MHD description for $\beta > 1$ and oblique propagation. Compressive solitons were shown to be unstable. Baumgärtel pointed out that this is consistent with considering the mirror mode instability as a driver creating both compressive and rarefactive wave structures where the instability of compressive waves subsequently allows only the magnetic holes to survive as they move into a mirror mode stable region. *Buti et al.* [2001], using a 1-D hybrid code, made the intriguing observation that not only are the compressive DNLS solitons unstable in the presence of density perturbations, but in their decay they collapse to a rarefactive wave structure resembling a magnetic hole. *Buti et al.* [1999] identified these density perturbations in a weakly nonlinear limit to behave as a sort of dissipation. With this mechanism they presented a new means through which magnetic holes might be formed. It is the purpose of this paper to elaborate on the connection between soliton theory and the magnetic hole formation mechanism found by *Buti et al.* [2001]. Following the spirit of *Hada et al.* [1993], we emphasize the value the IST can have in illuminating the nonlinear dynamics of Alfven waves in the presence of physical effects, such as dissipation, that go beyond the physics of the underlying DNLS soliton equation.

2. Derivative Nonlinear Schrodinger Equation

[6] The derivative nonlinear Schrodinger (DNLS) equation is found as the one-dimensional, weakly nonlinear and weakly dispersive limiting form of the equations of magnetohydrodynamics [*Landau et al.*, 1984] for wave travel parallel, or nearly parallel, to the ambient magnetic field. The DNLS equation may be written as

$$\frac{\partial b}{\partial t} + \alpha \frac{\partial}{\partial x}\left(|b^2|b\right) + iR\frac{\partial^2 b}{\partial x^2} = 0, \tag{1}$$

where R is the dispersion strength and $b(x, t) = B_y + iB_z$ with B_y and B_z being the components of the magnetic field transverse to a uniform, ambient magnetic field along the x axis. The value of α in the nonlinear term is given by [*Kennel et al.*, 1988]

$$\alpha = \frac{1}{4}\frac{v_A}{B_0^2}\frac{1}{1-\beta}, \quad \beta = \frac{c_S^2}{v_A^2}, \tag{2}$$

where v_A and c_S are the intermediate Alfven and sound speeds upstream and B_0 is the strength of the ambient magnetic field. Clearly then this model equation does not allow coupling between the Alfven and sound modes. While α is taken to be positive in this study, a kinetic derivation [*Khanna and Rajaram*, 1982] shows this choice to be consistent with $\beta > 1$ except in the vicinity of $\beta \approx 1$. It should be noted that models

based purely on fluid properties will overlook wave-particle interactions that arise in the case of finite beta. In a derivation starting from the Vlasov description *Rogister* [1971] found a model equation matching all the terms of the DNLS equation as well as a nonlinear, nonlocal term accounting for resonant particle effects. The same nonlinear term was found by *Mjolhus and Wyller* [1988] using a hybrid fluid and guiding-center method. *Flå et al.* [1989] used this nonlinear term to study the effect of resonant particles on parallel propagating, circularly polarized Alfven waves in a finite beta plasma and found it to produce wave damping and a decrease in large wave number features especially in left-hand polarized waves.

[7] While coupling to the sound mode is excluded, the DNLS equation does describe the coupling between the Alfvenic and magnetosonic modes that occurs in a plasma with $\beta < 1$ for wave propagation parallel, and nearly parallel, to the ambient magnetic field. The physical differences between parallel, $b(x, t) \rightarrow 0$ for $x \rightarrow \pm\infty$, and quasi-parallel or oblique, $b(x, t) \rightarrow b_0$ for $x \rightarrow \pm\infty$, wave travel are significant in the context of Alfven waves and are discussed in detail by *Hamilton et al.* [1992b] and *Mjolhus and Hada* [1997]. For $\beta < 1$, the Alfvenic and magnetosonic wave speeds coincide at parallel propagation and separate as the direction of wave travel moves away from parallel. At sufficiently large angles, the two modes decouple. For $\beta > 1$, the underlying MHD wave speeds remain close at any propagation angle [*Baumgärtel*, 1999]. *Ruderman* [2002] has shown that the DNLS description can be extended to large amplitude, oblique Alfven waves for a high-β plasma. This result is of importance in this paper as magnetic holes generally are oblique and tend to occur in high-β plasmas.

[8] For oblique waves it is convenient to shift to the Alfven wave frame of reference, in which case the DNLS takes the form

$$\frac{\partial b}{\partial t} + \frac{\partial}{\partial x}\left[\left(|b^2| - b_0^2\right)b\right] + i\frac{\partial^2 b}{\partial x^2} = 0, \tag{1'}$$

where b_o is the component of the ambient magnetic field perpendicular to the direction of wave propagation. Additionally, the equation has been scaled for convenience to set the nonlinear coefficient, α, as well as the dispersion coefficient, R, to be equal to one. The effects of weak Ohmic resistance have been modeled [*Mjolhus and Wyller*, 1988] through the derivative nonlinear Schrodinger-Burgers (DNLSB) equation:

$$\frac{\partial b}{\partial t} + \frac{\partial}{\partial x}\left[\left(|b^2| - b_0^2\right)b\right] + i\frac{\partial^2 b}{\partial x^2} = \bar{R}\frac{\partial^2 b}{\partial x^2}, \tag{3}$$

where $\bar{R}$ is the strength of the dissipation.

3. Inverse Scattering Transformation

[9] The IST method maps the DNLS, equation (1), onto a linear eigenvalue problem:

$$\Phi_x = D \cdot \Phi \text{ with } \Phi(\lambda; x, t) = \begin{pmatrix} \phi_{11} & \phi_{12} \\ \phi_{21} & \phi_{22} \end{pmatrix} \text{and}$$
$$D = \lambda \begin{pmatrix} -i\lambda & b(x,t) \\ \bar{b}(x,t) & i\lambda \end{pmatrix}, \tag{4a}$$

with time dependence given by

$$\Phi_t = F \cdot \Phi \text{ with } F(\lambda; x, t) = \begin{pmatrix} A & B \\ C & -A \end{pmatrix} \tag{4b}$$

[10] For the appropriate choice of A, B and C, the compatibility condition between equations (4a) and (4b), $\Phi_{xt} = \Phi_{tx}$, reduces to the DNLS equation (1).

[11] For parallel wave travel, $b(x, t) \rightarrow 0$ for $x \rightarrow \pm\infty$, the IST was developed by *Kaup and Newell* [1978]. For oblique waves, $b(x, t) \rightarrow b_0$ for $x \rightarrow \pm\infty$, the IST was developed by *Kawata and Inoue* [1978]. As the method and results for the oblique case are central to this study, they will be reviewed below.

[12] The appropriate choices for A, B and C of equation (4b) to yield the DNLS of equation (1′) are

$$A = 2i\lambda^4 + i\left(|b|^2 - b_0^2\right)\lambda^4$$
$$B = -2b\lambda^3 - \left[b\left(|b|^2 - b_0^2\right) + ib_x\right]\lambda$$
$$C = -2\bar{b}\lambda^3 + \left[-\bar{b}\left(|b|^2 - b_0^2\right) + i\bar{b}_x\right]\lambda \tag{5}$$

Given the nonvanishing boundary conditions, $b(x, t) \rightarrow b_0$ for $x \rightarrow \pm\infty$, *Kawata and Inoue* [1978] define two solutions of (4a) by

$$\Phi^{\pm}(\lambda, \zeta; x, t) \rightarrow T(\lambda, \zeta)J(\Lambda x) \text{ for } x \rightarrow \pm\infty,$$
$$\text{where } \Phi(\lambda, \zeta; x, t) = \begin{pmatrix} \phi_{11} & \phi_{12} \\ \phi_{21} & \phi_{22} \end{pmatrix}, \tag{6}$$

where

$$T(\lambda, \zeta) = \begin{pmatrix} -ib_0 & \lambda - \zeta \\ \lambda - \zeta & ib_0 \end{pmatrix}, J(\Lambda x) = \begin{pmatrix} e^{-i\Lambda x} & 0 \\ 0 & e^{+i\Lambda x} \end{pmatrix},$$
$$\Lambda = \lambda\zeta \text{ and } \zeta = \sqrt{\lambda^2 - b_0^2}.$$

These two are related to each other by

$$\Phi^{-}(\lambda, \zeta; x, t) = \Phi^{+}(\lambda, \zeta; x, t) \cdot S(\lambda, \zeta; t) \text{ with}$$
$$S(\lambda, \zeta; t) = \begin{pmatrix} s_{11} & s_{12} \\ s_{21} & s_{22} \end{pmatrix}, \tag{7}$$

where $S(\lambda, \zeta; t)$ is the scattering matrix. To demonstrate the meaning of the scattering coefficients, note the relation equation (7) creates between the left components of Φ^- and Φ^+:

$$\begin{pmatrix} \phi_{11}^- \\ \phi_{21}^- \end{pmatrix} = \begin{pmatrix} \phi_{11}^+ & \phi_{12}^+ \\ \phi_{21}^+ & \phi_{22}^+ \end{pmatrix} \cdot \begin{pmatrix} s_{11} \\ s_{21} \end{pmatrix}. \tag{8}$$

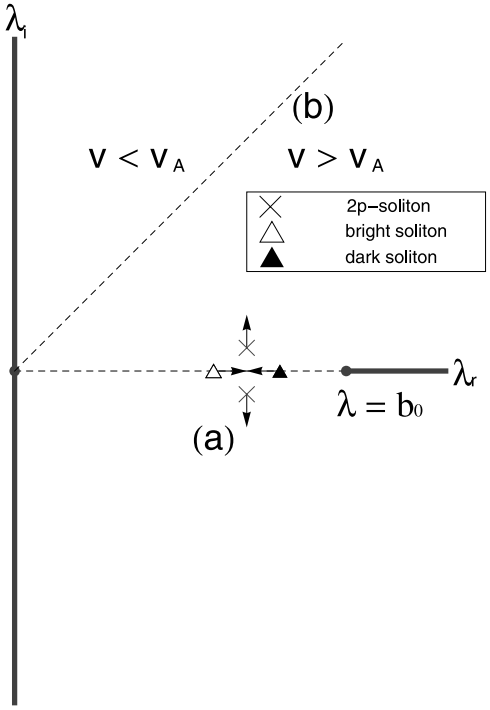

Figure 1. Complex λ plane showing eigenvalue regions for one-parameter and two-parameter solitons. Eigenvalues for one-parameter bright and dark solitons are real valued, scaled to the ambient field strength, and can exist for $0 < \lambda < b_0$, where $b_0 = B_x/B_0 = \mathrm{Cos}(\theta)$. Eigenvalues for two-parameter solitons are in complex conjugate pairs as shown. Amplitudes for all three soliton types decrease as $\mathrm{Re}(\lambda)$ approaches 0. For one-parameter solitons, as λ approaches b_o, amplitude decreases for a dark soliton and approaches a maximum for a bright soliton. (a) The allowed coalescence between a pair of bright and dark solitons resulting in the formation of a two-parameter soliton. (b) The complex plane divided into two regions corresponding to regions where the two-parameter soliton speed is faster or slower than the Alfven speed.

The eigenvalues occur when the solution to equation (4a) is bounded. From equations (6) and (8),

$$\begin{pmatrix}\phi_{11}^{-}\\ \phi_{21}^{-}\end{pmatrix} = \begin{pmatrix}-ib_0 & \lambda-\zeta\\ \lambda-\zeta & ib_0\end{pmatrix}\cdot\begin{pmatrix}e^{-i\Lambda x}\\ 0\end{pmatrix} = \begin{pmatrix}-ib_0e^{-i\Lambda x}\\ (\lambda-\zeta)e^{-i\Lambda x}\end{pmatrix}\rightarrow\begin{pmatrix}0\\0\end{pmatrix}$$

for $x \rightarrow -\infty$ if $\mathrm{Im}(\Lambda) > 0$. So $\begin{pmatrix}\phi_{11}^{-}\\ \phi_{21}^{-}\end{pmatrix}$ is bounded to the left. To the right, it is found that

$$\begin{pmatrix}\phi_{11}^{-}\\ \phi_{21}^{-}\end{pmatrix} = \begin{pmatrix}\phi_{11}^{+} & \phi_{12}^{+}\\ \phi_{21}^{+} & \phi_{22}^{+}\end{pmatrix}\cdot\begin{pmatrix}s_{11}\\ s_{21}\end{pmatrix} = \begin{pmatrix}-ib_0s_{11}e^{-i\Lambda x}+(\lambda-\zeta)s_{21}e^{+i\Lambda x}\\ (\lambda-\zeta)s_{11}e^{-i\Lambda x}+ib_0s_{21}e^{+i\Lambda x}\end{pmatrix}\rightarrow\begin{pmatrix}0\\0\end{pmatrix}$$

for $x \rightarrow +\infty$ if $\mathrm{Im}(\Lambda) > 0$ and $s_{11}(\lambda) = 0$. So $\begin{pmatrix}\phi_{11}^{-}\\ \phi_{21}^{-}\end{pmatrix}$ is bounded to both the left and right only where $s_{11}(\lambda) = 0$. The values λ_n for which this is the case are called eigenvalues and each one corresponds to a soliton for the wave profile b(x,t). In addition to the eigenvalues, another piece of information from the scattering matrix needed to construct a solution is the normalizing coefficient for each eigenvalue: $c_k = i\frac{s_{21}(\lambda_k)}{s_{11}'(\lambda_k)}$. Finally, there is the reflection coefficient: $\rho(\lambda) = \frac{s_{21}}{s_{11}}$. From (4b) and (5), the time dependence of the scattering data becomes

$$\rho(\lambda,t) = \rho(\lambda,0)\mathrm{Exp}\left(-4i\lambda^2\Lambda t\right),\ \lambda_k(t) = \lambda_k(0),\ \text{and}\ c_k(t) = c_k(0)\mathrm{Exp}\left(-4i\lambda^2\Lambda t\right).$$

As all the scattering data, or spectral data, are determined by $s_{11}(\lambda)$ and $s_{21}(\lambda)$ it is necessary to know how to evaluate these functions. They can be evaluated numerically as follows:

[13] 1. Numerically integrate equation (4a) using the initial magnetic field, b(x, t = 0), along with the defining asymptotics of equation (6) to solve for Φ^{-} (λ, ζ; x, t).

[14] 2. Use equation (7) to solve for $s_{11}(\lambda)$ and $s_{21}(\lambda)$ substituting Φ^{+} (λ, ζ; x, t) for its asymptotics of equation (6) for $x \rightarrow +\infty$.

[15] A single discrete eigenvalue corresponds to a nonlinear wave structure known as a soliton. The important point here is that any initial Alfven wave profile can be represented in terms of a nonlinear combination of its solitons and continuous spectrum. In the absence of any soliton part for an initial wave profile, the wave will then disperse away. In this sense, the nonlinear dynamics of Alfven waves are represented by the properties and interactions of its constituent solitons.

[16] For a system described precisely by the DNLS, the eigenvalues and any soliton property specified by them are independent of time. In the presence of additional physical effects, such as weak Ohmic resistance, the solitons become time dependent directly through the perturbing effects and indirectly through their interactions with other solitons and with the radiation component of the spectral data [*Kaup*, 1976; *Wyller and Mjolhus*, 1984]. The IST places general constraints on the means through which solitons, and their corresponding eigenvalues, can interact as well as how they can be created and destroyed [*Hamilton et al.*, 1992a]. These constraints arise from the analytic properties of the scattering data [*Kawata and Inoue*, 1978] which, for oblique Alfven waves, are analytic away from the branch cut, as shown in Figure 1, for $\mathrm{Re}(\lambda) > 0$. The constraints relevant to this study are summarized as follows:

[17] 1. A bright/dark soliton pair can coalesce to form a two-parameter soliton. In the complex eigenvalue plane this is seen as the real eigenvalues of the bright and dark solitons merge and subsequently move as a complex conjugate pair off the real axis. The converse of this process is also possible.

[18] 2. A soliton can diminish in amplitude becoming an algebraic soliton and subsequently becoming part of the continuous spectrum. For a two-parameter soliton this would be represented by $\mathrm{Re}(\lambda) \rightarrow 0$ or $\mathrm{Im}(\lambda) \rightarrow 0$ for $\mathrm{Re}(\lambda) > b_0$. For a one-parameter soliton, this would be represented by $\lambda \rightarrow 0$. Additionally, for a dark soliton as seen from Figure 1, this could also occur for $\lambda \rightarrow b_0$.

[19] 3. Coupling to the continuous spectrum can lead to the formation of an algebraic soliton which may be driven to become a one- or two-parameter soliton. The representation

of this in the complex plane is the converse of point 2 above.

4. Oblique Soliton Solutions of the DNLS Equation

[20] The distinctions between parallel and nonparallel waves, as described above, are reflected in the soliton solutions for the corresponding boundary conditions. For vanishing boundary conditions, the eigenvalues for equation (4a) can only be complex and the solitons in this case are referred to as two-parameter solitons. For nonvanishing boundary conditions there is additionally a possibility for real eigenvalues, referred to as one-parameter solitons. The one-parameter soliton solutions for the DNLS in this form can be written as [*Kawata and Inoue*, 1978; *Mjolhus and Hada*, 1997]

$$B_y = b_0 + \frac{2\lambda\eta^2 s}{b_0^2}\frac{(\mathrm{Cos}h(2\theta/\mathrm{L}) - \mathrm{b_0 s}/\lambda)}{(\mathrm{Cos}h(2\theta/\mathrm{L}) - \lambda \mathrm{s}/\mathrm{b_0})^2}$$
$$B_z = -\frac{2\eta^3 s}{b_0^2}\frac{\mathrm{Sin}h(2\theta/\mathrm{L})}{(\mathrm{Cos}h(2\theta/\mathrm{L}) - \lambda \mathrm{s}/\mathrm{b_0})^2} \tag{9}$$

where $\theta = x - ct$, $\eta = \sqrt{b_0^2 - \lambda^2}$, $c = 2\lambda^2$ and $L = {}^1/_{\lambda\eta}$ with $s = +1(-1)$ for a so-called bright (dark) soliton. Finally, λ is the eigenvalue for equation (4a) and is a real constant such that $0 < \lambda < b_0$.

[21] With the scaling as described above, the one-parameter soliton speed is given by $c = b_0^2 + 2\lambda^2$ with the value $\lambda = 0$ giving $c = b_0^2$, the Alfven wave speed, and ranging up to $\lambda = b_0$ giving $c = 3b_0^2$, the magnetosonic wave speed. That the one-parameter solitons exist only for oblique waves and that their speeds fill the range between the wave speeds of the Alfven and magnetosonic modes is an indication of the separation of the underlying wave speeds of these modes accompanied by the continued coupling between the modes.

[22] The two-parameter soliton for the DNLS equation was reported by *Mjolhus* [1989] on the basis of the IST results of *Kawata and Inoue* [1978]. From their results, the two-parameter soliton can also be written in the factored form of

$$b(x,t) = b_0\frac{[m\cdot n - (1+k)][\bar{f}\cdot\bar{g} - (1+k)]}{[f\cdot g - (1+k)]^2}, \tag{10}$$

where

$$f = 1 + \frac{e^{-i\phi}}{b_0 z_{10}} \quad g = 1 + \frac{e^{i\bar{\phi}}}{b_0 z_{01}}$$
$$\text{with } \phi = 2\Lambda\left[x - \left(b_0^2 + 2\lambda^2\right)t\right]$$
$$m = 1 + \frac{e^{-i\phi}}{b_0 d_{10}} \quad n = 1 + \frac{e^{i\bar{\phi}}}{b_0 d_{01}}$$
$$\text{and } \Lambda = \lambda\xi,\ \xi = \sqrt{\lambda^2 - b_0^2},\ k = -\left(\frac{\bar{\lambda}\xi + \lambda\bar{\xi}}{\bar{\lambda}\xi - \lambda\bar{\xi}}\right)^2$$
$$d_{10} = \left(\frac{\lambda - \xi}{b_0}\right)^2 z_{10} \quad d_{01} = \left(\frac{\bar{\lambda} + \bar{\xi}}{b_0}\right)^2 z_{01}$$
$$z_{10} = \frac{b_0(\lambda - \xi)}{2\Lambda\xi} \qquad z_{01} = \frac{b_0\left(\bar{\lambda} + \bar{\xi}\right)}{2\bar{\Lambda}\bar{\xi}}$$

The eigenvalue, λ, is complex and specifies all the properties of the soliton. For example, with $\lambda = \mu + i\nu$, the wave speed of the two-parameter soliton is $c = b_0^2 + 2(\mu^2 - \nu^2)$. Note that this speed can range higher and lower than both the Alfven and magnetosonic wave speeds.

5. Numerical Results

[23] Following the IST-based approach used by *Hada et al.* [1993] we present the results of a numerical study of the nonlinear dynamics of oblique Alfven waves subject to weak resistive damping. Soliton properties and their interactions are found to be central to the resulting nonlinear dynamics. Distinctive features observed are the formation of dark solitons through the damping of either bright or two-parameter solitons as well as the coalescence of bright and dark solitons to form two-parameter solitons.

[24] The weak damping of a two-parameter soliton leads to the formation of dark solitons as seen in Figures 2a–2c. The train of dark solitons is seen to the right in Figure 2a traveling with speeds above v_A. Also in Figure 2a, after a brief initial increase in amplitude, both the speed and amplitude of the two-parameter soliton can be seen to decrease as the soliton becomes a more oscillatory, longer wavelength structure that eventually will damp away. This corresponds to the Re(λ) becoming closer to zero, shown in Figure 2c. In Figure 2b it is seen that dark solitons, upon formation, are strongly affected initially reaching larger amplitudes and slower speeds as they quickly approach a final state. Finally, if the wave energy is defined as

$$E = \int_{-\infty}^{+\infty}\left(|b|^2 - b_0^2\right)dx, \tag{11}$$

then the time rate of change of total wave energy is found from the DNLSB, equation (3), to be [*Wyller and Mjolhus*, 1984]

$$\frac{\partial E}{\partial t} = -2\bar{R}\int_{-\infty}^{+\infty}\left|\frac{\partial b}{\partial x}\right|^2 dx < 0. \tag{12}$$

So the total wave energy must be decreasing at all times as is observed in Figure 2d.

[25] For the bright soliton it is seen in Figures 3a and 3b that weak damping leads to a continual increase in both the speed and amplitude of the soliton. Recalling that the speed of a one-parameter soliton is given by $c = b_0^2 + 2\lambda^2$ and that $c = b_0^2 + 2(\mu^2 - \nu^2)$ for a two-parameter soliton with $\lambda = \mu + i\nu$, Figure 2b shows that once the bright and dark soliton speeds match, they coalesce to form a two-parameter soliton traveling at a speed greater than $v_A = b_0^2$. The subsequent damping of such a two-parameter soliton results in decreasing speed and increasing amplitude until reaching the Alfven wave speed below which both amplitude and speed will continue to decrease. Formation of dark solitons begins as the speed nears the Alfven wave speed and continues until the soliton disperses away. Figure 3d shows that the overall wave energy is continually decreasing even when the energy of the bright or two-parameter soliton is increasing.

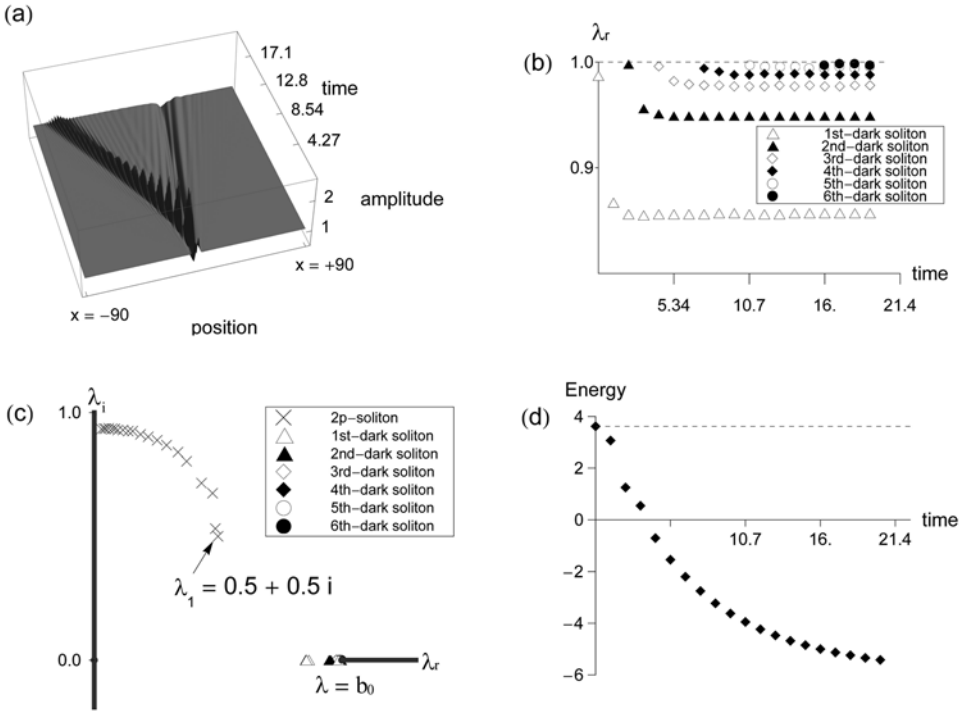

Figure 2. Damping of a two-parameter soliton: $\lambda_1 = 0.5 + 0.5i$. (a) Plot of amplitude as a function of position and time. The train of dark solitons is seen as the depression in the magnetic field amplitude traveling to the right ($v > v_A$), while the damped two-parameter soliton is seen with decreasing amplitude traveling to the left ($v < v_A$). (b) Graph of one-parameter soliton eigenvalues as a function of time. (c) Plot of the eigenvalue spectrum at fixed time intervals. (d) Plot of total energy at fixed time intervals. Here time is scaled to the inverse proton gyrofrequency, Ω_p^{-1}, and space is scaled to the proton inertial length, c/ω_{pi}.

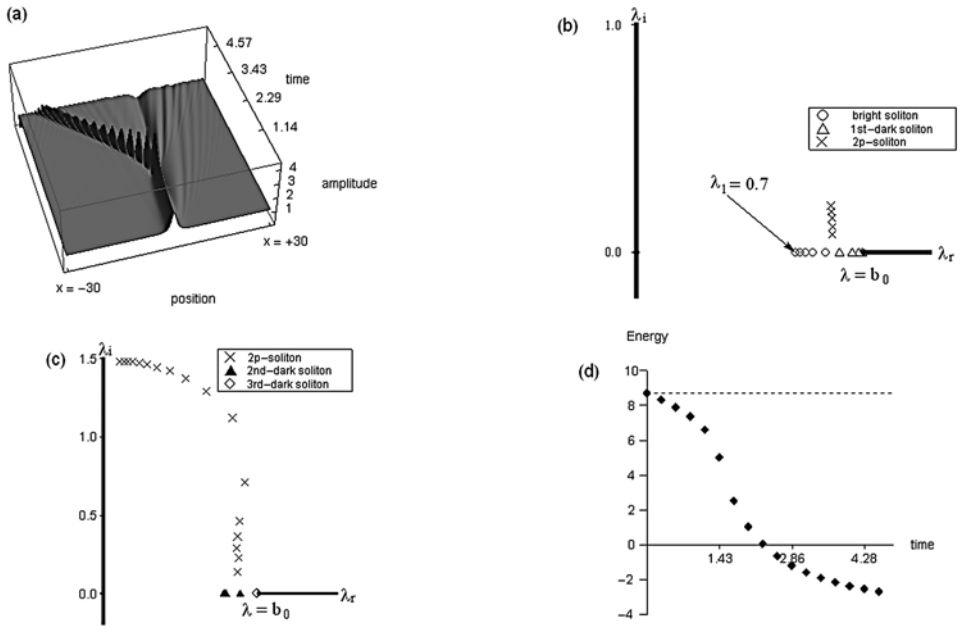

Figure 3. Damping of a bright one-parameter soliton: $\lambda_1 = 0.7$. (a) Plot of amplitude as a function of position and time. The train of dark solitons is seen as the depression in the magnetic field amplitude traveling to the right ($v > v_A$), while the damped two-parameter soliton is seen with decreasing amplitude traveling to the left ($v < v_A$). (b) Plot of the eigenvalue spectrum at fixed time intervals showing formation of the two-parameter soliton. (c) Plot of the eigenvalue spectrum at fixed time intervals starting just after formation of the two-parameter soliton. (d) Plot of total energy at fixed time intervals. Here time is scaled to the inverse proton gyrofrequency, Ω_p^{-1}, and space is scaled to the proton inertial length, c/ω_{pi}.

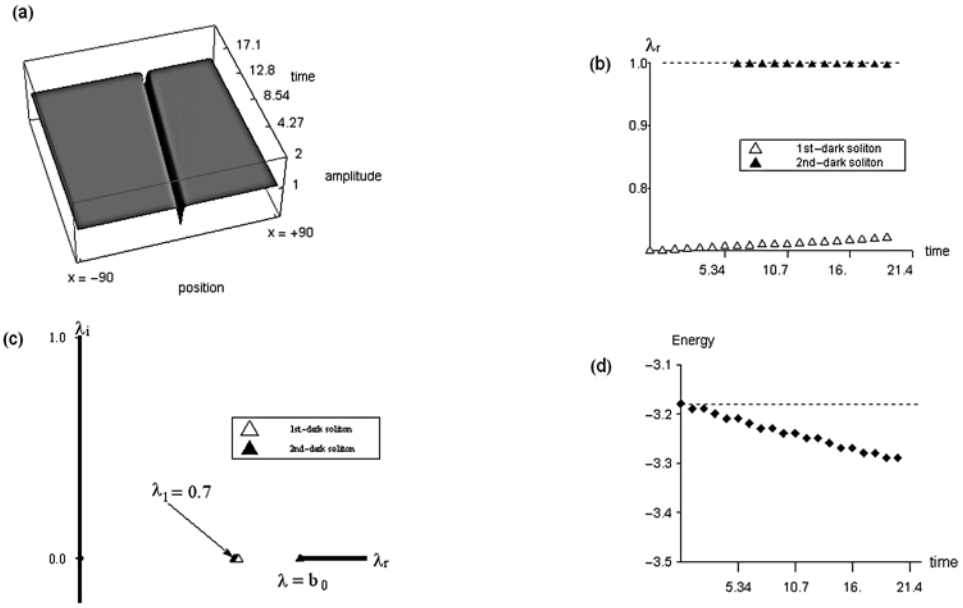

Figure 4. Damping of a dark one-parameter soliton: $\lambda_1 = 0.7$. (a) Plot of amplitude as a function of position and time. The initial dark soliton is seen as the depression in the magnetic field amplitude traveling to the right ($v > v_A$). (b) Graph of one-parameter soliton eigenvalues as a function of time. (c) Plot of the eigenvalue spectrum at fixed time intervals. (d) Plot of total energy at fixed time intervals. Here time is scaled to the inverse proton gyrofrequency, Ω_p^{-1}, and space is scaled to the proton inertial length, c/ω_{pi}.

[26] In Figure 2b it is seen that once a dark soliton reaches its final state, it is very weakly affected by dissipation. This is also seen in the damping of a lone dark soliton shown in Figures 4a–4d, where there is a slight tendency for the soliton speed to increase. The slight difference is that in the interaction with the two-parameter soliton, the dark solitons' speeds tended to decrease.

6. Discussion

[27] The inclusion of weak dissipation destroys the integrability of the DNLS equation and yet the nonlinear dynamics of Alfven waves modeled in this way are still seen to be organized around the dynamics and allowed interactions of the underlying solitons. Specifically, it is concluded on this basis that in the presence of weak Ohmic resistance an oblique Alfven wave with compressive solitons in its IST representation will inevitably yield a train of dark solitons. In the absence of either a compressive or rarefactive soliton component, the Alfven wave will dissipate away. The dark solitons formed will quickly reach a steady state in which they appear to be relatively weakly affected by both dissipation and by their interactions with each other. Magnetic holes have been tentatively identified as dark solitons and the results presented here, within the constraints of the DNLSB model discussed above, tend to support this role by giving an explanation for their widespread occurrence, their tendency to be observed in clusters and their persistence. In evaluating the relation between dark solitons and magnetic holes it would be worthwhile to clarify the conditions under which these solitons will be stable. It should be noted that *Ruderman* [1987], using a linear perturbation method, has shown dark solitons to be unstable to transverse perturbations, though this property has apparently not yet been investigated numerically.

[28] It would be valuable to determine the conditions and the extent to which nonlinear Alfven wave dynamics are usefully represented by the underlying soliton spectrum in the broader context of the Hall-MHD equations, 1-D hybrid-kinetic simulations and, ultimately, observations of magnetic holes in space. This could be done, in part, by a straightforward numerical study within Hall-MHD, or a hybrid simulation, through evaluation of the soliton spectrum as a function of time, as in Figures 3b and 3c, to determine if the underlying soliton dynamics follow the processes described above. It would seem difficult, but perhaps possible, to evaluate the evolution of the soliton spectrum during the formation of a magnetic hole through multipoint observations similar to those noted by *Stasiewicz et al.* [2003, 2004] using the Cluster spacecraft. An indirect observational test would be to evaluate the soliton spectrum of a single point observation of a magnetic compression associated with a train of magnetic holes, a relatively unusual feature noted by *Sperveslage et al.* [2000]. If the upstream compressional wave were the source of the train of magnetic holes then, by the simple model presented above, it should be identified in the soliton spectrum as containing a two-parameter soliton with $v < v_A$.

[29] Though the role of these results is uncertain for systems that are not near the DNLS description, some tentative support can be inferred for a degree of robustness from apparently conflicting 1-D hybrid code simulations [*Baumgärtel et al.*, 2003; *Buti et al.*, 2001] of compressive Alfven wave dynamics. It should be noted that the conditions of the simulations varied and also that both simulations were taken to be collisionless. The simulation of Buti *et al.* was intended to demonstrate the effects of field-density coupling

which had previously been shown [*Buti et al.*, 1999] to act as type of dissipation in a weakly nonlinear limit. Baumgärtel, using a compressive large amplitude, planar initial field profile, found that the wave eventually dispersed away. Buti, using a compressive large amplitude, left-hand polarized (as viewed from a stationary reference frame) initial field profile, found that the wave evolution eventually led to the formation of a large amplitude rarefactive wave. Within the IST perspective it has been established [*Hamilton et al.*, 1992b] that a planar, compressive profile does not have a soliton component and so should disperse away consistent with the results of Baumgärtel. Furthermore, only compressive, left-hand polarized profiles can contain compressive Alfven soliton components. It was found in section 5 that such compressive solitons will lead to the formation of rarefactive solitons in the presence of dissipation which is qualitatively consistent with the results of Buti. While the 1-D hybrid code simulations of Buti and Baumgärtel are in rough qualitative agreement with the IST-based predictions of this paper, it would be helpful in clarifying the extent of this agreement to evaluate the soliton components of the magnetic field profile at a sequence of times for these simulations.

[30] **Acknowledgments.** R.H. was supported by a research grant from George Fox University, R.H. and D.P. were supported by Holman funds through George Fox University, and S.L. was supported through the Richter Foundation.

[31] Amitava Bhattacharjee thanks Michael Stevens and another reviewer for their assistance in evaluating this paper.

References

Baumgärtel, K. (1999), Soliton approach to magnetic holes, *J. Geophys. Res.*, *104*(A12), 28,295–28,308, doi:10.1029/1999JA900393.

Baumgärtel, K., K. Sauer, and E. Dubinin (2003), Towards understanding magnetic holes: Hybrid simulations, *Geophys. Res. Lett.*, *30*(14), 1761, doi:10.1029/2003GL017373.

Baumgärtel, K., K. Sauer, and E. Dubinin (2005), Kinetic slow mode-type solitons, *Nonlinear Processes Geophys.*, *12*, 291–298.

Burlaga, L. F., N. F. Ness, and M. H. Acũna (2006), Trains of magnetic holes and magnetic humps in the heliosheath, *Geophys. Res. Lett.*, *33*, L21106, doi:10.1029/2006GL027276.

Buti, B., V. L. Galinski, V. I. Shevchenko, G. S. Lakhina, B. T. Tsurutani, B. E. Goldstein, P. Diamond, and M. V. Medvedev (1999), Evolution of nonlinear Alfven waves in streaming inhomogeneous plasmas, *Astrophys. J.*, *523*, 849–854, doi:10.1086/307743.

Buti, B., B. T. Tsurutani, M. Neugebauer, and B. E. Goldstein (2001), Generation mechanism for magnetic holes in the solar wind, *Geophys. Res. Lett.*, *28*(7), 1355–1358, doi:10.1029/2000GL012592.

Califano, F., P. Hellinger, E. Kuznetsov, T. Passot, P. L. Sulem, and P. M. Travnicek (2008), Nonlinear mirror mode dynamics: Simulations and modeling, *J. Geophys. Res.*, *113*, A08219, doi:10.1029/2007JA012898.

Erdos, G., and A. Balogh (1996), Statistical properties of mirror mode structures observed by Ulysses in the magnetosheath of Jupiter, *J. Geophys. Res.*, *101*(A1), 1–12, doi:10.1029/95JA02207.

Flå, T., E. Mjolhus, and J. Wyller (1989), Nonlinear Landau damping of weakly dispersive circularly polarized MHD waves, *Phys. Scr.*, *40*, 219–226, doi:10.1088/0031-8949/40/2/012.

Hada, T., R. L. Hamilton, and C. F. Kennel (1993), The soliton transform and a possible application to nonlinear Alfven waves in space, *Geophys. Res. Lett.*, *20*(9), 779–782, doi:10.1029/93GL00073.

Hamilton, R. L., C. F. Kennel, and E. Mjolhus (1992a), Stability and bifurcation of quasiparallel Alfvén solitons, *Phys. Scr.*, *46*, 230–236, doi:10.1088/0031-8949/46/3/005.

Hamilton, R. L., C. F. Kennel, and E. Mjolhus (1992b), Formation of quasiparallel Alfvén solitons, *Phys. Scr.*, *46*, 237–247, doi:10.1088/0031-8949/46/3/006.

Kaup, D. J. (1976), A perturbation expansion for the Zakharov-Shabat inverse scattering transform, *SIAM J. Appl. Math.*, *31*(1), 121–133, doi:10.1137/0131013.

Kaup, D. J., and A. C. Newell (1978), An exact solution for a derivative nonlinear Schrödinger equation, *J. Math. Phys. N. Y.*, *19*, 798, doi:10.1063/1.523737.

Kawata, T, and H. Inoue (1978), Exact solution of the derivative nonlinear Schrodinger equation under the nonvanishing conditions, *J. Phys. Soc. Jpn.*, *44*, 1968–1976, doi:10.1143/JPSJ.44.1968.

Kennel, C. F., B. Buti, T. Hada, and R. Pellat (1988), Nonlinear, dispersive, elliptically polarized Alfven waves, *Phys. Fluids*, *31*(7), 1949–1961, doi:10.1063/1.866642.

Khanna, M., and R. Rajaram (1982), Evolution of nonlinear Alfven waves propagating along the magnetic field in a collisionless plasma, *J. Plasma Phys.*, *28*(3), 459–468.

Kivelson, M. G., and D. J. Southwood (1996), Mirror instability II: The mechanism of nonlinear saturation, *J. Geophys. Res.*, *101*(A8), 17,365–17,371, doi:10.1029/96JA01407.

Landau, L. D., E. M. Lifshitz, and L. P. Pitaevskii (1984), *Electrodynamics of Continuous Media*, 2nd ed., 460 pp., Pergamon, New York.

Mjolhus, E. (1989), Nonlinear Alfvén waves and the DNLS equation: Oblique aspects, *Phys. Scr.*, *40*, 227–237, doi:10.1088/0031-8949/40/2/013.

Mjolhus, E. (2006), Velocity-amplitude relationships and polarizations in families of MHD solitary waves, *Phys. Scr. T*, *122*, 135, doi:10.1088/0031-8949/2006/T122/017.

Mjolhus, E., and T. Hada (1997), Soliton theory of quasi-parallel MHD waves, in *Nonlinear Waves and Chaos in Space Plasmas*, edited by T. Hada and H. Matsumoto, pp. 121–169, Terra Sci., Tokyo.

Mjolhus, E., and J. Wyller (1988), Nonlinear Alfven waves in a finite-beta plasma, *J. Plasma Phys.*, *40*(2), 299–318.

Pantellini, F. G. E. (1998), A model of the formation of stable nonpropagating magnetic structures in the solar wind based on the nonlinear mirror instability, *J. Geophys. Res.*, *103*(A3), 4789–4798, doi:10.1029/97JA02384.

Pokhotelov, O. A., R. Z. Sagdeev, M. A. Balikhin, O. G. Onishchenko, and V. N. Fedun (2008), Nonlinear mirror waves in non-Maxwellian space plasmas, *J. Geophys. Res.*, *113*, A04225, doi:10.1029/2007JA012642.

Rogister, A. (1971), Parallel propagation of nonlinear low-frequency waves in high-β plasma, *Phys. Fluids*, *14*, 2733–2739, doi:10.1063/1.1693399.

Ruderman, M. S. (1987), Stability of quasilongitudinally propagating solitons in a plasma with Hall dispersion, *Izv. Akad. Nauk SSSR, Mekh. Zhidkisti Gaza*, *2*, 159–165.

Ruderman, M. S. (2002), DNLS equation for large-amplitude solitons propagating in an arbitrary direction in a high-β plasma, *J. Plasma Phys.*, *67*(4), 271–276, doi:10.1017/S002237780200168X.

Russell, C. T., W. Riedler, K. Schwingenschuh, and Y. Yeroshenko (1987), Mirror instability in the magnetosphere of Comet Halley, *Geophys. Res. Lett.*, *14*(6), 644–647, doi:10.1029/GL014i006p00644.

Sperveslage, K., F. M. Neubauer, K. Baumgärtel, and N. F. Ness (2000), Magnetic holes in the solar wind between 0.3 AU and 17 AU, *Nonlinear Processes Geophys.*, *7*, 191–200.

Stasiewicz, K. (2004), Theory and observations of slow-mode solitons in space plasmas, *Phys. Rev. Lett.*, *93*(12), 125004, doi:10.1103/PhysRevLett.93.125004.

Stasiewicz, K., P. K. Shukla, G. Gustafson, S. Buchert, B. Lavraud, B. Thide, and Z. Klos (2003), Slow magnetosonic solitons detected by the Cluster spacecraft, *Phys. Rev. Lett.*, *90*(8), 085002, doi:10.1103/PhysRevLett.90.085002.

Sugiura, M., T. L. Skillman, B. Ledley, and J. P. Heppner (1969), "Holes" in the magnetic field near the magnetopause, *Eos Trans. AGU*, *50*, 278.

Tsurutani, B. T., E. J. Smith, R. R. Anderson, K. W. Ogilvie, J. D. Scudder, D. N. Baker, and S. J. Bame (1982), Lion roars and nonoscillatory drift mirror waves in the magnetosheath, *J. Geophys. Res.*, *87*(A8), 6060–6072, doi:10.1029/JA087iA08p06060.

Tsurutani, B. T., D. J. Southwood, E. J. Smith, and A. Balogh (1992), Nonlinear magnetosonic waves and mirror mode structures in the March 1991 Ulysses interplanetary event, *Geophys. Res. Lett.*, *19*(12), 1267–1270, doi:10.1029/92GL00782.

Tsurutani, B. T., B. Dasgupta, C. Galvan, M. Neugebauer, G. S. Laknina, J. K. Arballo, D. Winterhalter, B. E. Goldstein, and B. Buti (2002a), Phase-steepened Alfven waves, proton perpendicular energization and the creation of magnetic holes and magnetic decreases: The ponderomotive force, *Geophys. Res. Lett.*, *29*(24), 2233, doi:10.1029/2002GL015652.

Tsurutani, B. T., C. Galvan, J. K. Arballo, D. Winterhalter, R. Sakurai, E. J. Smith, B. Buti, G. S. Lakhina, and A. Balogh (2002b), Relationship between discontinuities, magnetic holes, magnetic decreases, and nonlinear Alfven waves: Ulysses observations over the solar poles, *Geophys. Res. Lett.*, *29*(11), 1528, doi:10.1029/2001GL013623.

Tsurutani, B. T., G. S. Lakhina, J. S. Picket, F. L. Guarnieri, N. Lin, and B. E. Goldstein (2005), Nonlinear Alfven waves, discontinuities, proton perpendicular acceleration, and magnetic holes/decreases in interplanetary space and the magnetosphere: Intermediate shocks?, *Nonlinear Processes Geophys.*, *12*, 321–336.

Turner, J. M., L. F. Burlaga, N. F. Ness, and J. F. Lemaire (1977), Magnetic holes in the solar wind, *J. Geophys. Res.*, *82*, 1921–1924, doi:10.1029/JA082i013p01921.

Winterhalter, D., M. Neugebauer, B. E. Goldstein, E. J. Smith, S. J. Bame, and A. Balogh (1994), Ulysses field and plasma observations of magnetic holes in the solar wind and their relation to the mirror-mode structures, *J. Geophys. Res.*, *99*, 23,371–23,381, doi:10.1029/94JA01977.

Winterhalter, D., E. J. Smith, M. Neugebauer, B. E. Goldstein, and B. T. Tsurutani (2000), The latitudinal distribution of solar wind magnetic holes, *Geophys. Res. Lett.*, *27*(11), 1615–1618, doi:10.1029/1999GL003717.

Wyller, J., and E. Mjolhus (1984), A perturbation theory for Alfven solitons, *Physica D*, *13*, 234–246, doi:10.1016/0167-2789(84)90280-X.

R. L. Hamilton, S. M. Libby, and D. A. Peterson, Department of Engineering, Math and Computer Science, George Fox University, P.O. Box 6125, 414 North Meridian, Newberg, OR 97132, USA. (rhamilton@georgefox.edu)